Supporting Information

In-situ X-Ray Absorption Spectroscopy (XAS) Investigation of a Bifunctional Manganese Oxide Catalyst with High Activity for Electrochemical Water Oxidation and Oxygen Reduction

Yelena Gorlin,[a†] Benedikt Lassalle-Kaiser,[b†] Jesse D. Benck,[a] Sheraz Gul,[b] Samuel M. Webb,[c] Vittal K. Yachandra,[b] Junko Yano,[b*] Thomas F. Jaramillo[a*]

[a]Department of Chemical Engineering Stanford University, Stanford, CA 94305
[b]Physical Biosciences Division, Lawrence Berkeley National Laboratory Berkeley, CA 94720
[c]Stanford Synchrotron Radiation Lightsource, SLAC National Accelerator Laboratory, Menlo Park, CA, 94025

[†]These authors contributed equally to the work
*Corresponding authors, E-mail: jyano@lbl.gov, jaramillo@stanford.edu

X-ray Photoelectron Spectroscopy Analysis

To monitor changes in the Mn oxidation state of MnO_x catalyst, we compared the distance between Mn $2p_{1/2}$ peak and its satellite ($\Delta 2p_{1/2}$) and the magnitude of Mn 3s multiplet splitting ($\Delta E3s$). To extract information from Mn 3s, the spectra were analyzed using CasaXPS software. Curves were fit using a Shirley background and 70% Gaussian 30% Lorentzian line shapes. To determine the magnitude of 3s multiplet splitting, we needed to de-convolute Au 4f spectrum from Mn 3s spectrum. In the analysis, we fixed the splitting distance between Au $4f_{7/2}$ and Au $4f_{5/2}$ to be 3.7 eV and the ratio of Au $4f_{7/2}$ peak area to Au $4f_{5/2}$ peak area to be 1.33.

Table S1. XPS Acquisition Parameters.

XPS Region	Energy (eV)	# of Scans
C 1s	275-310	130
Mn 2p	632-675	260
Mn 3s	75-105	260

X-ray Absorption Spectroscopy Experimental Details

Curve fitting was performed with Artemis and IFEFFIT software using *ab initio*-calculated phases and amplitudes from the program FEFF 8.2.[1,2] These *ab initio* phases and amplitudes were used in the EXAFS equation:

$$\chi(k) = S_0^2 \sum_j \frac{N_j}{kR_j^2} f_{eff_j}(\pi,k,R_j) e^{-2\sigma_j^2 k^2} e^{-2R_j/\lambda_j(k)} \sin(2kR_j + \phi_{ij}(k)) \quad (1)$$

The neighboring atoms to the central atom(s) are divided into j shells, with all atoms with the same atomic number and distance from the central atom grouped into a single shell. Within each shell, the coordination number N_j denotes the number of neighboring atoms in shell j at a distance of R_j from the central atom. $f_{eff_j}(\pi,k,R_j)$ is the *ab initio* amplitude function for shell j, and the Debye-Waller term $e^{-2\sigma_j^2 k^2}$ accounts for damping due to static and thermal disorder in absorber-backscatterer distances. The mean free path term $e^{-2R_j/\lambda_j(k)}$ reflects losses due to inelastic scattering, where $\lambda_j(k)$ is the electron mean free path. The oscillations in the EXAFS spectrum are reflected in the sinusoidal term, $\sin(2kR_j + \varphi_{ij}(k))$ where $\varphi_{ij}(k)$ is the *ab initio* phase function

for shell *j*. S_0^2 is an amplitude reduction factor due to shake-up/shake-off processes at the central atom(s). The EXAFS equation was used to fit the experimental data using *N*, *R*, and the EXAFS Debye-Waller factor (σ^2) as variable parameters. For the energy (eV) to wave vector (*k*, $Å^{-1}$) axis conversion, E_0 was defined as 6545.0 eV and the S_0^2 value was fixed to 0.85. All fits were performed in the R space.

Table S2: Mineral name, formula, and oxidation state of MnO_x phases.

Mineral name	Formula	Individual oxidation states	Average oxidation state
Manganosite	MnO	II	2
Hausmannite	Mn_3O_4	II, III, III	2.7
Bixbyite	α-Mn_2O_3	III, III	3
Manganite	γ-MnOOH	III	3
M^{n+}-Birnessite	M^{n+}-MnO_2[a]	III, IV	3.7[3,4]
M^{n+}-Hollandite	M^{n+}-$(Mn^{III}Mn^{IV})_8O_{16}$[a]	III, IV	3.8[5]
M^{n+}-Todorokite	M^{n+}-$(Mn^{III}Mn^{IV})_6O_{12}\cdot 3.5H_2O$[a]	III,IV	3.7[5]
Pyrosulite	β-MnO_2	IV	4

[a]M^{n+} = Mg^{2+}, K^+, Na^+, Ba^+, H^+, etc. The oxidation state of these phases will depend on the preparation route.

Table S3: XANES linear combination fitting of the 1.8V OER catalyst.

	9C (%)			1C (%)	
Birnessite	80.5	83.2	84.2	83.3	93.1
Mn_3O_4	13.9	16.8	-	-	6.9
Mn_2O_3	5.6	-	15.8	16.7	-
R factor	0.0021	0.0021	0.0023	0.0056	0.0054

The error of these numbers (%) is ~ 5%. R factor was obtained by $\Sigma(\text{data-sum})^2/\Sigma(\text{data})^2$.

Discussion of Electrochemical Activity of Mn_3O_4

In heterogeneous catalysis, one of the most challenging endeavors is to unequivocally identify active sites. While one cannot completely discount the possibility that the Mn_3O_4 phase contributes to OER activity, we believe that the less oxidized Mn_3O_4 phase is unlikely to be driving the OER at 1.8 V vs. RHE. In electrocatalysts such as MnO_x, the oxidation is believed to be confined to the surface layer and

some of the film is expected to remain un-oxidized and electrochemically inactive.[6] Therefore, in our schematic (Figure 8), we show the most likely scenario where Mn_3O_4 is located in the interior of the film, away from electrode-electrolyte interface. An alternative explanation is that some Mn_3O_4 remains on the surface in contact with electrolyte and is not hidden in the interior of the film. Because the thermodynamic potential for Mn_3O_4 oxidation is 0.7 V vs. RHE,[7] while the thermodynamic potential for OER is 1.23 V vs. RHE, under OER conditions (1.8 V vs. RHE) an overpotential of 1.1 V exists for the oxidation of Mn_3O_4 and 0.57 V for the OER. Considering the greater overpotential for the oxidation of Mn_3O_4 and the fact that both the OER and Mn_3O_4 oxidation requires a reaction with OH^-,[8] we can conclude that if Mn_3O_4 was electrically connected to the electrode it would likely oxidize prior to reaching 1.8 V. Because we can detect Mn_3O_4 in our measurements under OER conditions, any Mn_3O_4 located on the catalytic surface and in contact with electrolyte must be electronically isolated (for example, as part of the film that has peeled off or as isolated particles that have poor contact to the rest of the film) and cannot turn over electrochemical water oxidation. This interpretation is consistent with previous literature that has shown Mn_3O_4 to have poor electrical conductivity and reversibility.[9,10]

Table S4: EXAFS curve fitting parameters.

	Fit#	Path	R (Å)	N	σ^2 (Å^2)	R (%)
Mn_3O_4[a]		Mn-O	1.95	**4**	0.005	0.3
		Mn-O	2.26	**2**	0.009	ΔE_0=4.58
		Mn-Mn	2.90	**2**	0.004	
		Mn-Mn	3.12	**4**	0.004	
		Mn-Mn	3.43	**4**	0.004	
		Mn-Mn	3.83	**2**	0.006	
0.7 V MnO_x	1[b]	Mn-O	1.90	**6**	0.013	7.4
		Mn-Mn	2.90	**6**	0.024	ΔE_0=-3.5
	2[a]	Mn-O	1.98	4.0	**0.005**	3.2
		Mn-O	2.28	2.0	**0.009**	ΔE_0=9.94
		Mn-Mn	2.94	1.9	**0.004**	
		Mn-Mn	3.17	3.8	**0.004**	
		Mn-Mn	3.43	1.8	**0.004**	
		Mn-Mn	3.97	0.9	**0.006**	
birnessite[c]		Mn-O	1.90	**6**	0.006	1.5
		Mn-Mn	2.88	**6**	0.009	ΔE_0=5.2
		Mn-O	3.41	**4**	0.004	
		Mn-O-Mn	3.84	**6**	0.005	
1.8 V MnO_x[c]	1	Mn-O	1.88	4.9	**0.006**	1.2
		Mn-Mn	2.85	3.6	**0.009**	ΔE_0=1.2
		Mn-O	3.52	1.8	**0.004**	
		Mn-O-Mn	3.76	1.2	**0.005**	
	2	Mn-O	1.87	**6**	0.007	5.0
		Mn-Mn	2.85	**6**	0.013	ΔE_0=-0.2
		Mn-O	3.53	**4**	0.009	
		Mn-O-Mn	3.80	**6**	0.015	

[a] Mn_3O_4 and 0.7 V MnO_x data were fit in the k-range of 2.9 < k (/Å) < 11.1 (1.0 < R (Å) < 3.8). In fit 2, the ratio between N values for the short and long Mn-O, Mn-Mn and Mn-Mn (Tetragonal) was set to be identical to that in

Mn_3O_4. [b]The 0.7 V MnO_x data were fit in the k-range of 2.9 < k (/Å) < 11.1 (0.7 < R (Å) < 2.64). [c]Birnessite and 1.8 V MnO_x data were fit in the k-range of 3.1 < k (/Å) < 11.4 (1.0 < R (Å) < 3.9 Å).

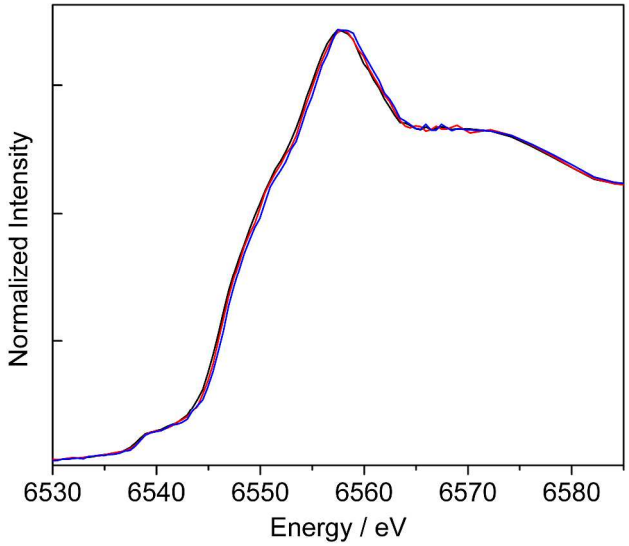

Figure S1. First (red) and fourth (blue) sets (average of 20 QXAS scans) and average (black, dash-dot) XANES spectra of the MnOx film poised at 0.7 V.

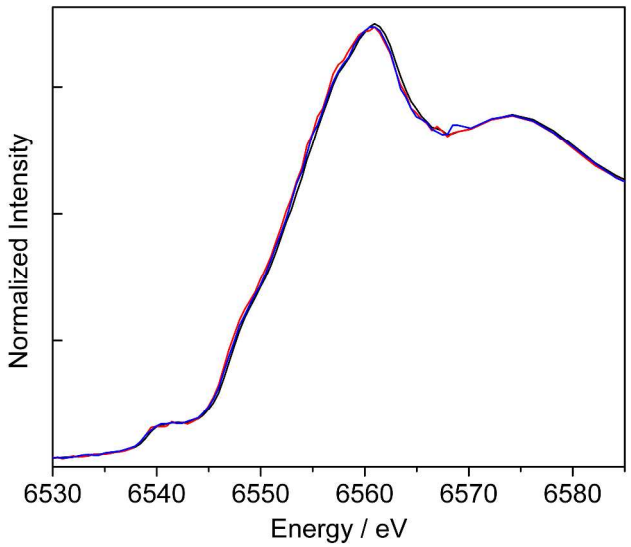

Figure S2. First (red) and fourth (blue) sets (average of 20 QXAS scans) and average (black, dash-dot) XANES spectra of the MnO_x film poised at 1.8 V.

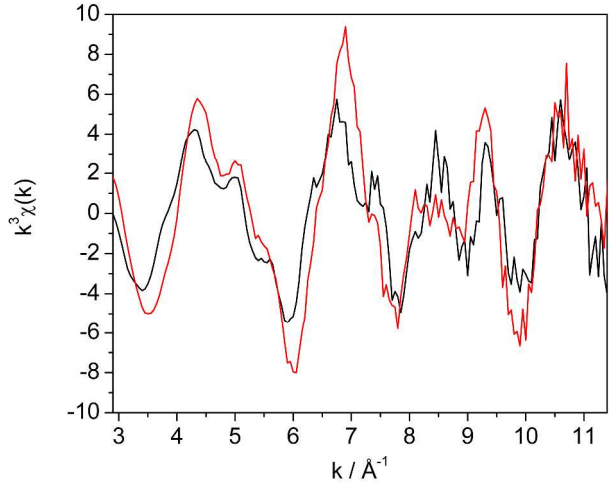

Figure S3. k^3 weighted EXAFS signal for the MnO_x film poised at 0.7 V (black) and 1.8 V (red). The range shown is that used for the EXAFS fittings.

X-ray Diffraction of MnO_x Powder Standards

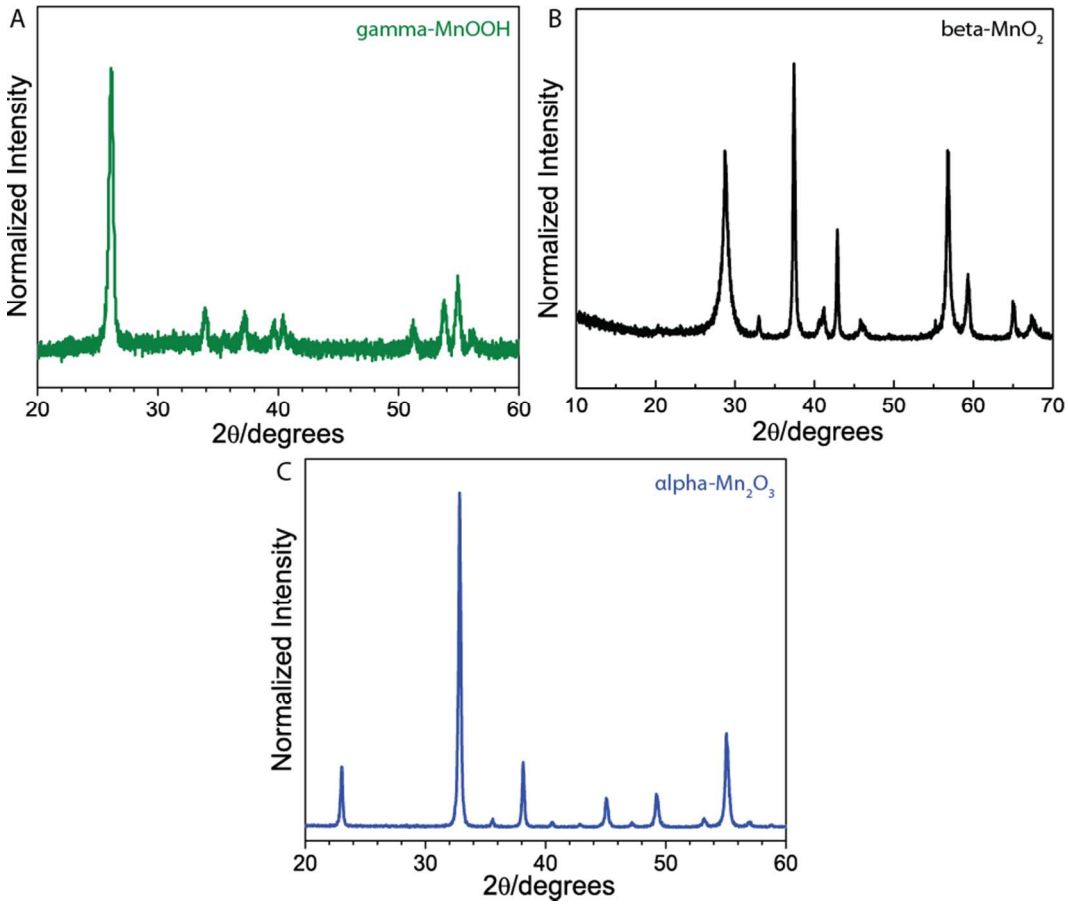

Figure S4. X-ray diffraction confirming A. gamma-MnOOH, B. alpha-Mn_2O_3, and C. beta-MnO_2 phases of powders used as dry standards in x-ray absorption spectroscopy (XAS) experiments.

Electrochemical Activity of MnO_x/Au-Si_3N_4 and MnO_x/GC Catalysts

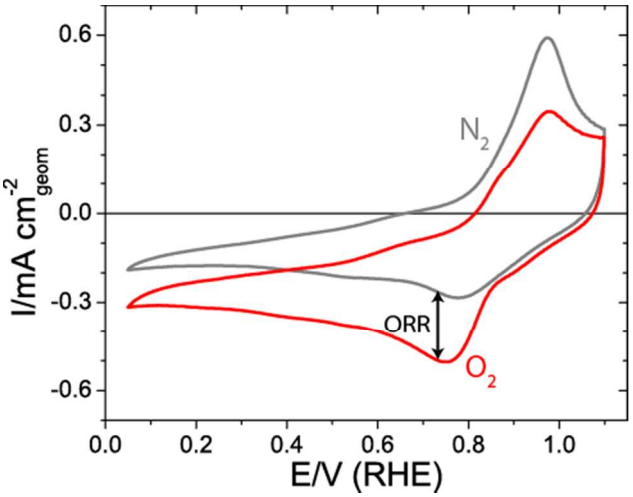

Figure S5. Electrochemical characterization of MnO_x/Au-Si_3N_4 in nitrogen and oxygen saturated electrolytes. The arrow indicates an increase in the reductive current upon addition of oxygen, confirming that the catalyst has significant oxygen reduction reaction activity.

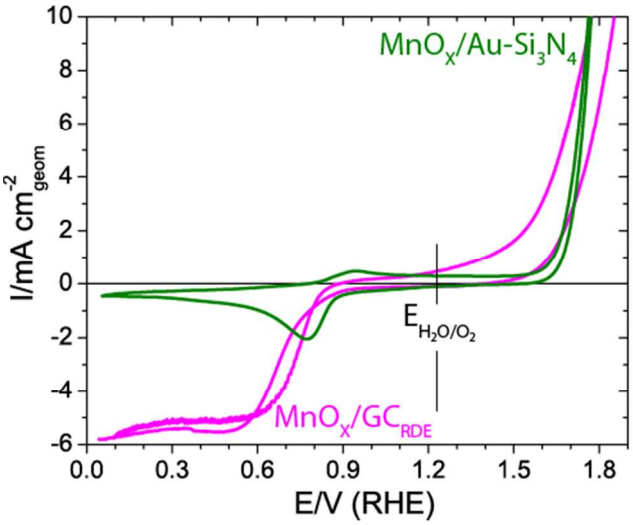

Figure S6. Comparison of oxygen reduction and evolution activities of manganese oxide on gold coated silicon nitride window (MnO_x/Au-Si_3N_4) and manganese oxide on glassy carbon rotating disk electrode substrate (MnO_x/GC_{RDE}); the oxygen reduction activity of MnO_x/GC_{RDE} reaches greater currents at higher overpotential values due to increased mass transfer of O_2 in RDE configuration (1600 revolutions per minute rotation).

X-ray Diffraction of MnO_x/Au-Si_3N_4 and MnO_x/GC Catalysts

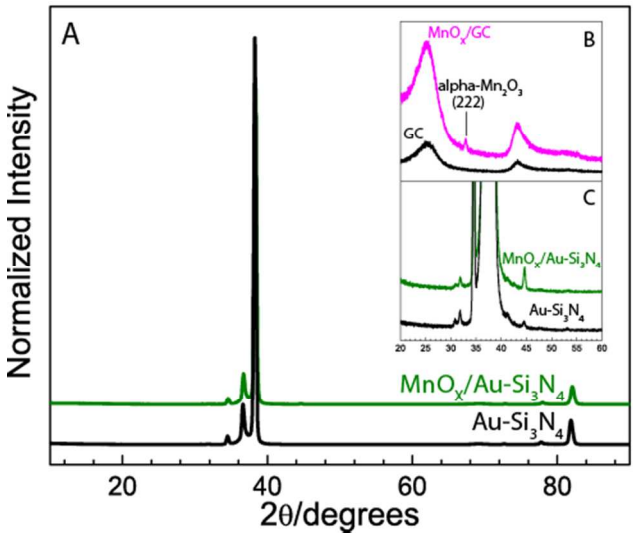

Figure S7. A. X-ray diffraction spectra of MnO_x/Au-Si_3N_4 catalyst and Au-Si_3N_4 support demonstrates that the catalyst has diffraction peaks characteristic to gold and gold oxide only. Inset B shows the x-ray diffraction spectra of glassy carbon (GC) support and MnO_x/GC catalyst, demonstrating alpha-Mn_2O_3 crystallinity of MnO_x/GC catalyst. The y-axis of inset C is magnified 100 times with respect to the y-axis of A to observe any minor peaks in MnO_x/Au-Si_3N_4 catalyst and Au-Si_3N_4 support.

X-ray Photoelectron Spectroscopy Characterization

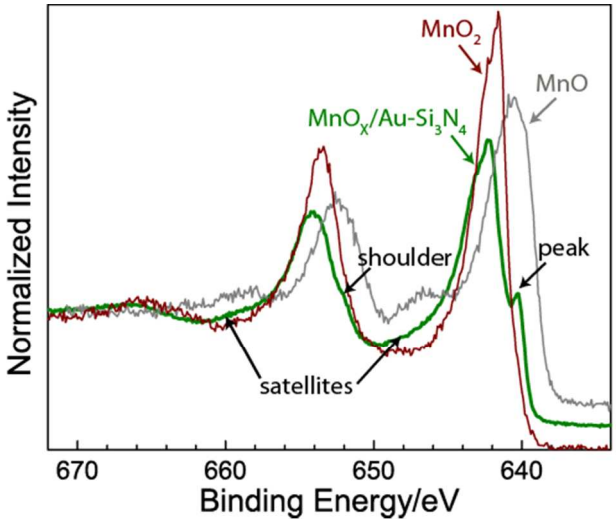

Figure S8. X-ray photoelectron spectra of MnO_x/Au-Si_3N_4 compared to the spectra of two powder controls: MnO and MnO_2. Arrows point out the features corresponding to MnO phase.

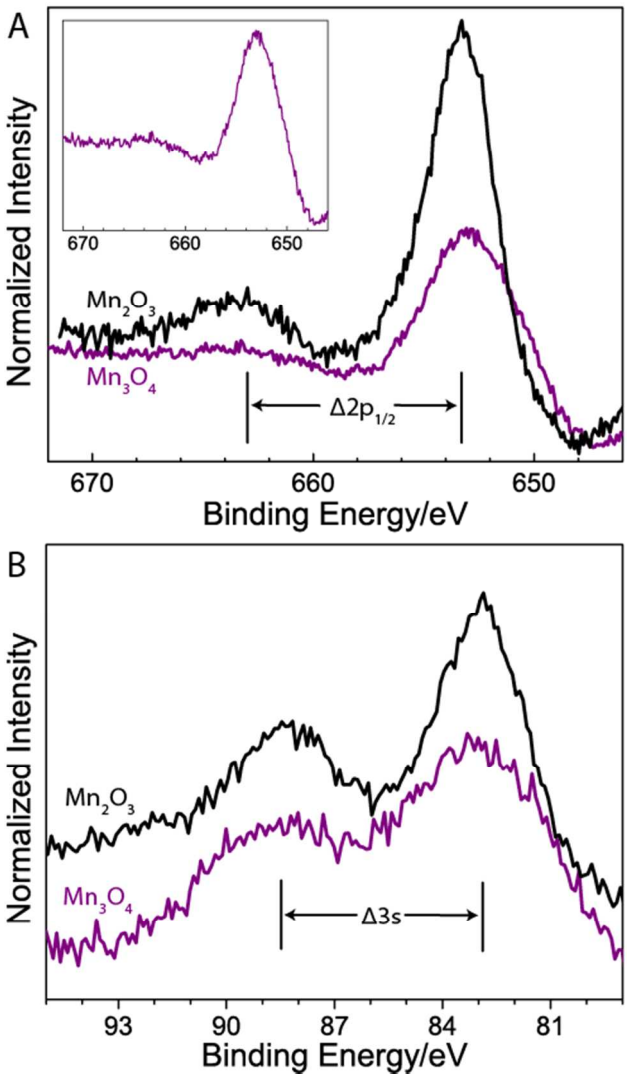

Figure S9. Comparison of x-ray photolectron spectra of Mn_2O_3 and MnOOH powder controls in A. Mn 2p region and B. Mn 3s region.

XANES Spectra of MnO_x Powder Standards

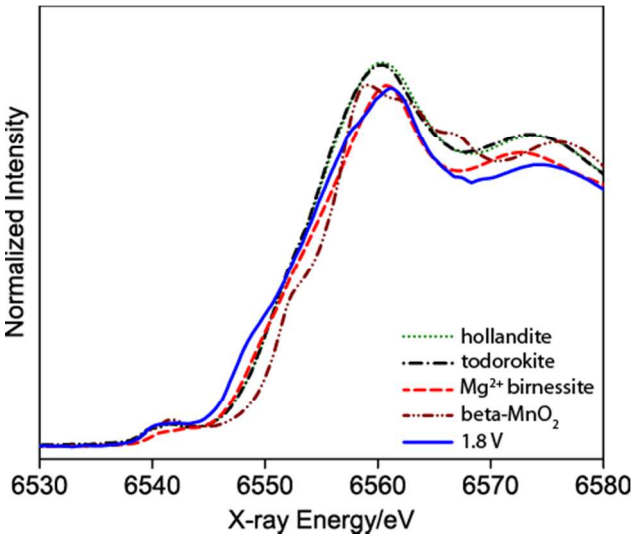

Figure S10. Comparison of XANES spectra of of hollandite and todorokite, which have been published and made available by Manceau et al,[5] to the spectra of Mg^{2+} birnessite, beta-MnO^2, and MnO_x/Au-Si_3N_4 poised at 1.8 V.

K 2p X-ray Photoelectron Spectra

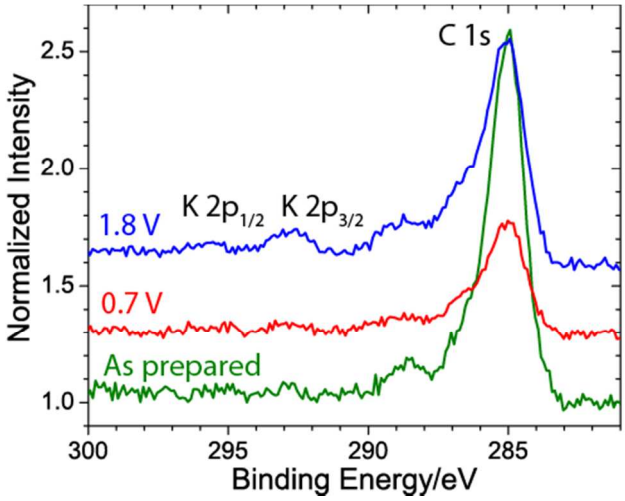

Figure S11. XPS spectra of MnO_x /$AuSi_3N_4$ film as deposited, after applying 0.7 V, and 1.8 V. In 1.8 V sample, two new peaks appear at ca. 294 eV and 297.5 eV that correspond to K $2p_{1/2}$ and K $2p_{3/2}$, respectively.

References

(1) Newville, M. *J. Synchrotron Radiat.* **2001**, *8*, 96.

(2) Rehr, J. J.; Albers, R. C. *Rev. Mod. Phys.* **2000**, *72*, 621.

(3) Ching, S.; Petrovay, D. J.; Jorgensen, M. L.; Suib, S. L. *Inorg. Chem.* **1997**, *36*, 883.

(4) Golden, D. C.; Chen, C. C.; Dixon, J. B. *Clays Clay Miner.* **1987**, *35*, 271.

(5) Manceau, A.; Marcus, M. A.; Grangeon, S. *Am. Mineral.* **2012**, *97*, 816.

(6) Nam, K.-W.; Kim, K.-B. *J. Electrochem. Soc.* **2006**, *153*, A81.

(7) Pourbaix, M. *Atlas of Electrochemical Equilibria in Aqueous Solutions*; Pergamon Press, 1966.

(8) Djurfors, B.; Broughton, J. N.; Brett, M. J.; Ivey, D. G. *J. Electrochem. Soc.* **2006**, *153*, A64.

(9) Boden, D.; Venuto, C. J.; Wisler, D.; Wylie, R. B. *J. Electrochem. Soc.* **1968**, *115*, 333.

(10) McBreen, J. *Electrochim. Acta* **1975**, *20*, 221.